ABSTRACT

Title of Document: NEW ELECTROLYTE AND ELECTRODE MATERIALS FOR USE IN LITHIUM- ION BATTERIES

Veidhes R. Basrur, Master of Science, 2010

Directed by: Prof. Srinivasa R. Raghavan & Prof. Chunsheng Wang
Department of Chemical & Biomolecular Engineering

Lithium-ion batteries have emerged as the preferred type of rechargeable batteries, but there is a need to improve the performance of the electrolytes and electrodes therein. Here, we report studies on new electrolyte and anode materials for use in such batteries.

First, we report a class of gel electrolytes prepared by utilizing the synergistic interactions between a molecular gelator, 1,3:2,4-di-O-methylbenzylidene-D-sorbitol (MDBS), and a nano-scale particulate material, fumed silica (FS). When MDBS and FS are combined in a liquid electrolyte of propylene carbonate and lithium perchlorate, the liquid is converted into a free-standing gel due to the formation of a strong MDBS-FS network. The gel exhibits an elastic shear modulus ~ 1000 kPa and a yield stress around 15 kPa – both values far exceed those obtainable by MDBS or FS alone in the same liquid. The electrolyte also shows high conductivity (~ 5×10^{-3} S/cm), a wide electrochemical stability window (up to 4.5 V), and good interfacial stability with lithium electrode.

In the second study, we describe a new polymeric binder [(poly (acryl amide-co-acrylic acid)] for use in conjunction with silicon (Si) anodes. This binder was combined with Si particles to form composite anode materials, which were then subjected to galvanostatic charge-discharge tests. Capacities exceeding 1000 mAh/g after 120 cycles have been obtained depending on the molecular weight of the binder and the concentration of the Si particles. The above binder thus presents a viable alternative to carboxymethyl cellulose (CMC), which is the current benchmark binder material for Si anodes.

New Electrolyte and Electrode Materials for Use in Lithium-Ion Batteries

Veidhes Basrur

Thesis submitted to the Faculty of the Graduate School of the
University of Maryland, College Park, in partial fulfillment
Of the requirements for the degree of
Master of Science
2010

Advisory Committee:

Prof. Srinivasa R. Raghavan

Prof. Chunsheng Wang

Prof. Sheryl H. Ehrman

Prof. Gregory S. Jackson

Dedication

This thesis is dedicated to my family for their unconditional love, the immense efforts they took for ensuring a good education for me and encouraging me in every task that I undertook.

Acknowledgements

I would like to thank Dr. S. Raghavan and Dr. C. Wang for the opportunity to join their research groups and giving me challenging projects to work on. I also greatly appreciate the concern they showed for my work in the lab as well as about my career. They encouraged me not only with words but also by their actions. It was a real pleasure to work with you.

In particular, I would like to acknowledge Dr. Hee-Young Lee who would never hesitate to take time out of his busy schedule to help me with any of my doubts and Dr. Juchen Guo who helped me get acquainted with a lot of difficult concepts and complex procedures with infinite patience even when he was busy. I would also like to thank to all my group members – Dr.Matt Dowling, Dr. Kunshan Sun, Dr. Rakesh Kumar, Vishal Javvaji, Hyuntaek Oh, Charles Kuo – whose company was sheer fun and who were always helpful when I needed to bounce some ideas.

Last but in no way the least, I want to acknowledge my Mamma, Pappa, my baby sister and all my friends back home whose unwavering support has got me through all the tough times in my life.

TABLE OF CONTENTS

Chapter 1: INTRODUCTION & OVERVIEW

This thesis is centered on the subject of *lithium-ion batteries*. Lithium-ion batteries fall under the category of rechargeable batteries. As the name suggests, these batteries function by the transport of Li^+ ions from the anode to the cathode during discharging and back again during charging. Lithium-ion (Li-ion) batteries are now commonly used in consumer electronics. They are a very popular choice for portable electronic goods like laptops and mobile phones. This is because of their high energy density and low self-discharge. These batteries have also been applied in hybrid-electric vehicles and in aerospace applications. Figure 1.1 shows examples of different lithium ion batteries available in the market. Their ability to be processed in such a variety of shapes and sizes is one of the reasons for their popularity.

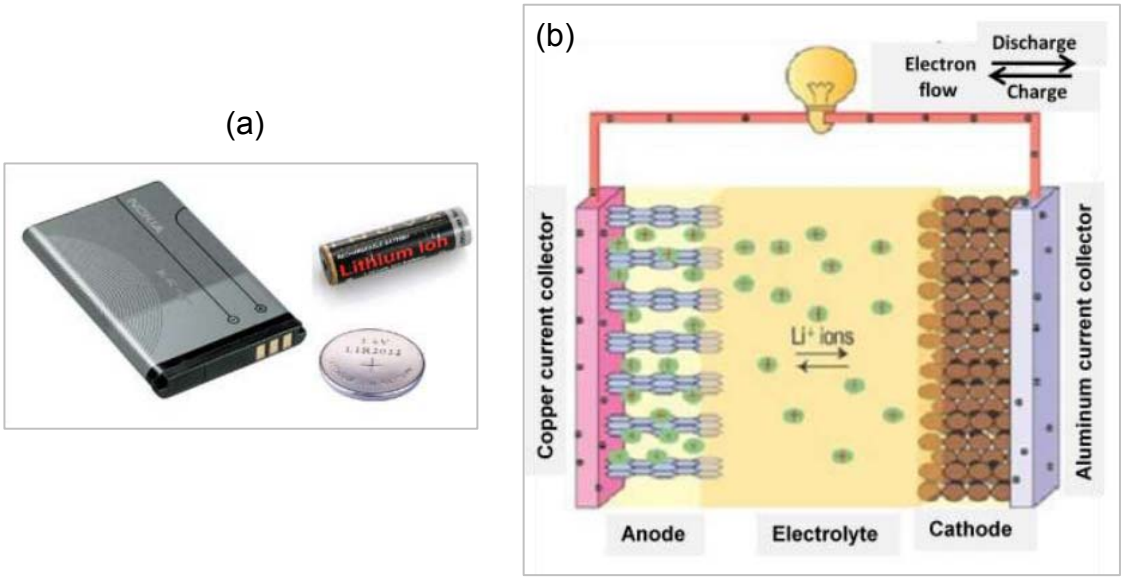

Figure 1.1 (a) Examples of lithium-ion batteries. **(b)** Schematic of a lithium-ion battery.[1]

Figure 1.1b is a schematic showing the operation of a Li-ion cell. When the cell is being discharged, Li^+ ions are transported from the anode to the cathode through the non-aqueous electrolyte and the porous separator membrane. On the other hand, when the discharged cell is being recharged, an external power source is used to apply a higher voltage than that produced by the battery, albeit in the opposite direction. Under these conditions, Li^+ ions migrate from the cathode to the anode. The electrode materials are both lithium intercalation compounds. Intercalation cathodes include lithium cobalt oxide ($LiCoO_2$), lithium iron phosphate ($LiFePO_4$) or lithium manganese oxide ($LiMn_2O_4$). Typical intercalation anodes are manufactured from carbon, specifically graphite. The electrolytes used are non-aqueous because lithium is very reactive with water producing lithium hydroxide and hydrogen gas, which is explosive. The function of the porous membrane separator is to prevent physical contact between the electrodes, thereby ensuring that the cell does not short-circuit.

Li-ion batteries have numerous advantages over other rechargeables. They are much lighter than other rechargeables that have equivalent energy capacities. They possess a high open-circuit voltage when compared to batteries such as lead acid, nickel cadmium (Ni-Cd) and nickel-metal hydride (Ni-MH). This is advantageous as it allows the delivery of increased power at a lower current. Li-ion batteries do not show any "memory effect", unlike Ni-Cd batteries: i.e., when a Ni-Cd battery is repeatedly discharged and charged to a partial extent, it appears to "remember" this point and adopts this new smaller capacity as its deliverable capacity. The self-discharge rate of Li-ion

batteries is also very small: i.e., if the battery is stored without use for a long time, it retains the bulk of its stored charge.

Researchers are evaluating various ways to improve the performance of Li-ion batteries, and this provides the motivation for the current thesis. With respect to the anode, materials like silicon, tin, and germanium are being considered as alternatives to graphite because these materials have higher capacities. Silicon has potential capacity which is 10 times that of graphite but one major problem with using silicon as an anode is its accompanying volume expansion which destroys the anode eventually. This problem demands the use of a binder capable of accommodating the silicon volume change. *One of the focuses of this thesis is to investigate the use of Poly (acryl amide-co-acrylic acid) as a binder to enhance the performance of the* ***silicon*** *anodes*.

The electrolyte in Li-ion batteries has also been a subject of much research. Typical electrolytes consist of a mixture of a lithium salt in a polar organic solvent. The main disadvantage of liquid electrolytes relates to the safety and durability of the batteries. There is the danger of thermal runaway and the potential threat of explosion. Also, liquid electrolytes pose leakage risks. Thus, added safety measures have to be installed in Li-ion batteries for tackling overheating and internal pressure relief, which together add to the cost of production. An ideal electrolyte would have the mechanical stability of a solid but also the conductivity of a liquid. *A second focus of this thesis is to prepare a new type of gelled electrolyte that combines good mechanical strength and high conductivity. The electrolyte is prepared by the self-assembly of a molecular gelator*

together with a class of nano-scale particles. The objective of such a mechanically strong electrolyte is:

- To prevent risk of leakage
- To avoid build up of internal pressure
- Reduce the cost by reducing the number of added safety measures

Chapter 2: BACKGROUND

In this chapter, we discuss basic aspects pertaining to the key components of lithium-ion (Li-ion) batteries, i.e., the anode, cathode and electrolyte. Thereafter, we briefly describe the various characterization techniques used in this study, specifically rheology and electrochemical impedance spectroscopy (EIS).

2.1. ANODES

The electrode where oxidation of a species (in this case Li) occurs is referred to as the anode. At the anode, Li loses electrons and gets transferred into the electrolyte solution as Li^+ during the discharge cycle. The reverse occurs during the charging of the battery, i.e., the Li^+ ions gain electrons and enter into the intercalation anode matrix. For a material to be a good anode it should posses certain characteristics. It should have a high capacity (charge storage ability) and low irreversible capacity, which means that every time it undergoes cycling the capacity-loss should be as low as possible. It should have a very low Li insertion potential (70–100mV). It should also possess a long cycle life and be electrochemically stable with the other components and materials in the cell. For Li-ion batteries, one material that possesses most of the above properties is graphite. It has a reversible capacity of 372 mAh/g and it is stable with Li metal. It can sustain a cycle life of at least 800-1000 cycles. All these properties have led to the commercialization of graphite anodes. Figure 2.1 portrays the mechanism of graphite anode operation.

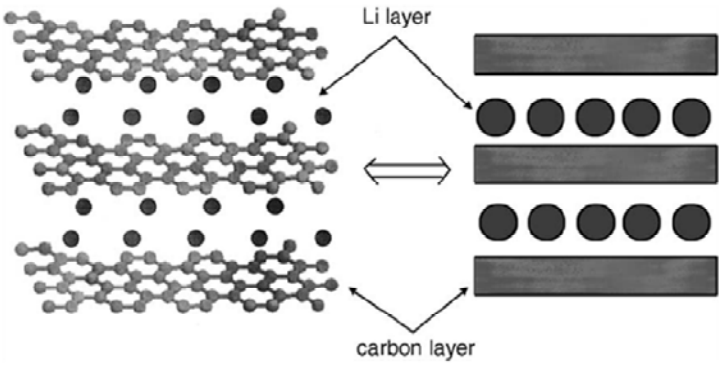

Figure 2.1. Schematic showing the intercalation of Li between the layers of graphite.[2]

In comparison to graphite, silicon (Si), germanium (Ge) and other Group 4 compounds posses much higher theoretical capacities as Li intercalation anodes (e.g., Si = 3975 mAh/g, Ge = 1624 mAh/g)[3]. However, they perform very poorly on cycling and show a very fast capacity fade, due to their brittle structure. The brittleness issue in the case of Si is explained in Figure 2.2. The large extent of Li insertion is accompanied by a large volume change of the Si matrix, which causes the structure to break after a few cycles. These breaks reduce the contact between the Si matrix and the current collector and thereby contribute to a loss in capacity.

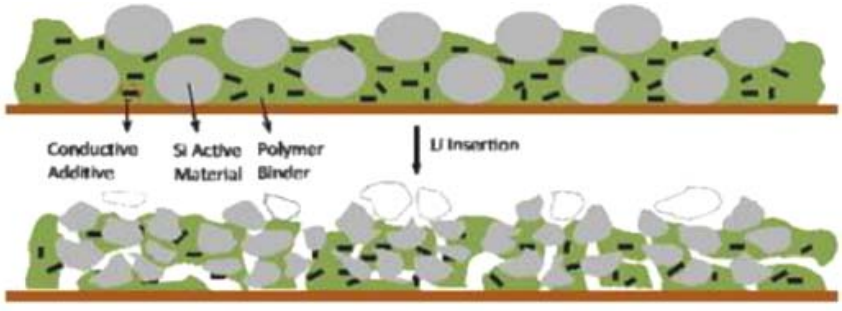

Figure 2.2. Poor performance of silicon anodes due to their brittleness upon Li insertion.

2.2. CATHODE

The cathode is the electrode at which reduction of a species occurs. During the discharge process, Li^+ ions gain electrons and intercalate into the cathode. During charge, Li atoms lose their electrons and go back into the electrolyte. The properties necessary for a good cathode are similar to those required of an anode, i.e., high capacity, low irreversible capacity, long cycle life and good electrochemical stability with the battery components. It should also have a high lithium insertion potential (> 3.5-4 V). Figure 2.3 depicts the structure of typical intercalation cathodes, such as manganese spinel [$LiMn_2O_4$] and lithium iron phosphate ($LiFePO_4$).

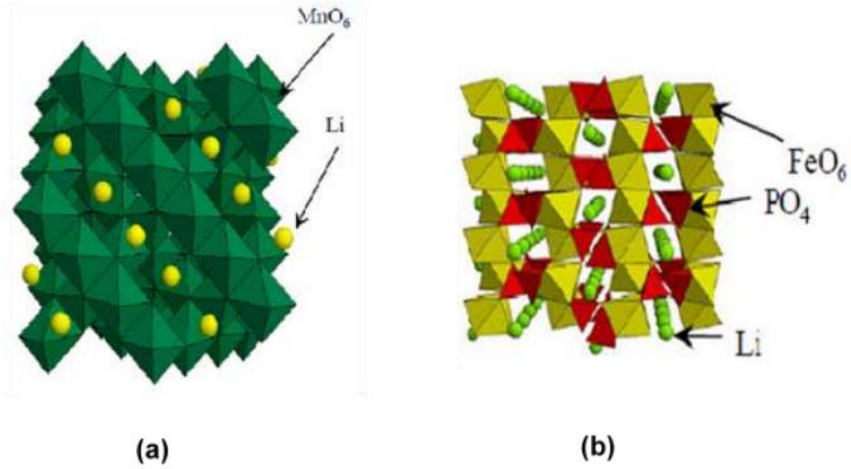

Figure 2.3. Structures of intercalation cathodes: **(a)** lithium manganese oxide ($LiMn_2O_4$) and **(b)** lithium iron phosphate ($LiFePO_4$). [4]

2.3. ELECTROLYTES

The electrolyte is the material that conducts ions between the electrodes. When the battery is being discharged, oxidation occurs at the anode, generating electrons. Since electrons cannot pass through the electrolyte, they go through the external circuit towards the cathode, thereby constituting an electric current. These electrons are neutralized at the

cathode due to the reduction reaction of the ions which arrive from the electrolyte. Thus the external circuit is completed by the internal transfer of ions from anode to cathode. In this fashion chemical energy is converted into electrical energy.

The characteristics of a good electrolyte are: a wide and stable electrochemical window, an ionic conductivity > 10^{-3} S/cm at the operating temperature, and an electronic conductivity < 10^{-10} S/cm so that electrons find the route through the external circuit to be the path of least resistance. The electrolyte should also be chemically stable with the electrodes and possess the ability to rapidly form a passivating solid-electrolyte interface layer to minimize the effect of interfacial resistance. The electrolyte must also ideally be non-flammable, non-explosive in the event of a short-circuit, nontoxic and cheap.

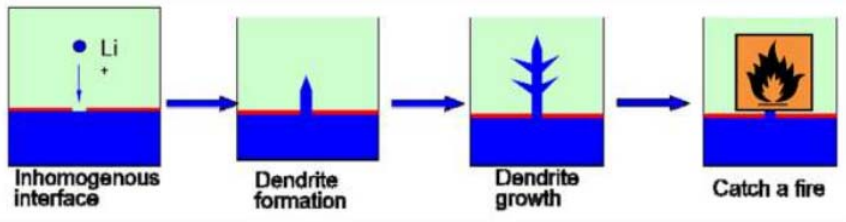

Figure 2.4. Lithium dendrite formation in the electrolyte, causing fire hazards.

As previously mentioned, Li reacts vigorously with water, which rules out the use of aqueous electrolytes in Li-ion batteries. So Li-ion batteries employ polar organic liquids like propylene carbonate (PC), ethylene carbonate (EC) etc. These organic liquids possess flash points below 30°C and are flammable. In the case of liquid electrolytes, continuous cycling of Li^+ in the battery may imply that some of the ions do not insert back into the electrodes; instead, the ions may deposit as dendrites (Figure 2.4)

emanating typically from the anode surface. If these dendrites touch the cathode, the cell short-circuits and the resulting sparks may cause the electrolyte to explode.

To avoid some of the safety problems with liquid electrolytes, researchers have studied polymer gel electrolytes or solid polymer electrolytes (SPEs). The use of solid materials ensures no leakage of the electrolyte from the cell. Also, the dendrite problem is better controlled or eliminated with SPEs. However, SPEs, which are high-molecular weight polymers, generally have very low conductivities at room temperature. Polymer gel electrolytes are usually made by swelling a polymeric matrix with a solvent. Their conductivities are better, but the presence of liquid in the matrix can still be problematic.

2.4. RHEOLOGY

This section attempts to give a basic understanding of rheology – a scientific discipline of vital importance to the study of soft materials such as gels, polymers, emulsions, and foams. Rheology is defined as the study of flow behavior and deformation in various materials. It is particularly useful in characterizing *viscoelastic* materials – i.e., those that possess a combination of viscous and elastic properties. Rheological measurements are typically performed under steady or dynamic shear. In steady shear, the sample is subjected to a constant shear-rate $\dot{\gamma}$ (e.g. by applying a continuous rotation at a fixed rate on a rotational instrument), and the response is measured as a shear-stress σ. The ratio of shear-stress σ to shear-rate $\dot{\gamma}$ is the (apparent) viscosity η. A plot of the viscosity vs. shear-rate $\dot{\gamma}$ is called the flow curve of the material.

Rheological experiments can also be conducted in dynamic or oscillatory shear, where a sinusoidal strain $\gamma = \gamma_0 \sin(\omega t)$ is applied to the sample. Here γ_0 is the strain-amplitude (i.e. the maximum applied deformation) and ω is the frequency of the oscillations. The sample response will be in the form of a sinusoidal stress $\sigma = \sigma_0 \sin(\omega t + \delta)$ which will be shifted by a phase angle δ with respect to the strain waveform. Using trigonometric identities, the stress waveform can be decomposed into two components, one in-phase with the strain and the other out-of-phase by 90°:

$$\sigma = G'\gamma_0 \sin(\omega t) + G''\gamma_0 \cos(\omega t) \tag{2.1}$$

where G' is the **Elastic** or **Storage Modulus** and G'' is the **Viscous** or **Loss Modulus**.

The physical meanings of the two moduli are as follows. The elastic modulus G' provides information about the elastic nature of the material. Since elastic behavior implies the storage of deformational energy, this parameter is also called the storage modulus. The viscous modulus G'', on the other hand, characterizes the viscous nature of the material. Since viscous deformation results in the dissipation of energy, G'' is also called the loss modulus. For these properties to be meaningful, the dynamic rheological measurements must be made in the "*linear viscoelastic*" (LVE) regime of the sample. This means that the stress must be linearly proportional to the imposed strain (i.e., moduli independent of strain amplitude). In that case, the elastic and viscous moduli are only functions of the frequency of oscillations ω. A log-log plot of the moduli vs. frequency, i.e. $G'(\omega)$ and $G''(\omega)$, is called the frequency spectrum of the material and represents a signature of the material microstructure.

The linear viscoelastic moduli reflect the microstructures present in the sample at rest. For an elastic or gel-like material, the elastic modulus G' (ω) is nearly constant, and its value is a measure of the *stiffness* of the gel. With regard to the *strength* of the gel, it is useful to characterize the variation of G' as a function of the strain-amplitude γ_0 at a fixed frequency. The value of γ_0 at which G' begins to plummet (i.e., the sample yields), is termed the yield strain γ_y. The product $G' \times \gamma_y$ is then the yield stress σ_y of the sample and is an overall measure of gel strength.

2.5. ELECTROCHEMICAL IMPEDANCE SPECTROSCOPY (EIS)

In EIS, an alternating (AC) potential $E = E_0 \exp(j\omega t)$ is applied to an electrochemical cell and the AC current $I = I_0 \exp(j\omega t - \varphi)$ through the cell is measured. The impedance Z of the cell is then represented as:

$$Z(\omega) = \frac{E}{I} = Z_0 \exp(j\varphi) = Z_0 (\cos\varphi + j \sin\varphi) \tag{2.2}$$

As seen from eq 2.2, the impedance has a real and an imaginary part. If the real part is plotted on the x-axis and the imaginary part on the y-axis, we get a Nyquist plot. This plot is then mapped on to an equivalent circuit made up of standard electrical components (resistor, capacitor, inductor etc), which is assumed to model the behavior of the electrochemical cell being tested. Here, we have used EIS to measure the conductivity of our gel electrolytes.

Chapter 3: NEW HYBRID ELECTROLYTES BY SYNERGISTIC GELATION OF FUMED SILICA AND A SORBITOL-BASED MOLECULAR GELATOR

3.1. INTRODUCTION

The limitations of conventional liquid electrolytes for lithium-ion (Li-ion) batteries are well known. Liquids can leak out of the batteries, which is particularly a concern because these electrolytes are typically based on flammable organic solvents.[5-7] Also, such electrolytes can interact adversely with the electrodes, leading to dendrites or an interfacial layer that adds a large electrical resistance. In turn, these factors compromise the long-term stability and safety of liquid-based Li-ion batteries.

It has long been recognized that solid polymer electrolytes (SPEs) could solve many of the above concerns with liquid electrolytes. Polymer manufacturing and processing operations are also well established in industry, which could facilitate commercialization of SPE-based cells. Also, solid polymer batteries may potentially be created in a variety of new configurations, including thin films, sheets, or rolls. These aspects have motivated extensive research into SPEs, especially into high molecular weight poly (ethylene oxide) (PEO) doped with Li salts.[8-11] However, these SPEs showed low room-temperature ionic conductivities, typically $<10^{-5}$ S/cm.[11-13] For most practical applications at room temperature, an ionic conductivity $>10^{-3}$ S/cm is essential.

Researchers have therefore sought ways to obtain electrolytes with solid-like character, but with liquid-like ionic conductivities. In addition, an ideal electrolyte should

also exhibit low interfacial resistances at the electrodes, which indicates stable cycling performance. The electrolyte should also exhibit a high value of the Li^+ ion transference number, which reflects the fraction of the total current that is carried by that ion (the closer this fraction is to 1 the better).

One way tried to achieve the above set of properties has been to start with a solvent or oligomeric liquid and then convert it to a gel by adding an appropriate gelling agent.[14-15] The use of the low molecular-weight solvent ensures a high ionic conductivity in the presence of Li salts, provided the gel network has large enough pores to allow free diffusion of solvent and ions. Thus, the salient feature of gel-electrolytes is that ionic mobility (and hence conductivity) is decoupled from the gel matrix. This is unlike SPEs wherein the ions have to hop along from one polymer chain to another and therefore conductivity is determined by the flexibility and molecular weight of the polymer.

Among the gelling agents used to create gel-electrolytes, we will consider two in this study. The first is fumed silica (FS), which is a form of silica with branched clusters and nano-scale primary particles.[15-17] By tuning the surface chemistry of the silica for a given solvent, it is possible to induce the silica particles to cluster into a three-dimensional fractal network.[18-21] The resulting gels have shear moduli around 100 kPa, but they are thixotropic, i.e., the application of shear liquefies the gels, although the gel-like character is regained after shear is stopped. Thus, the gels are not strong enough to be used as true solids, i.e., without a porous membrane separator. To increase the mechanical strength of the above gels, researchers have developed modified fumed silicas

with polymerizable methacrylate groups on their surface. Compositions with these modified silicas were crosslinked by ultraviolet (UV) light to give rubbery solids with improved mechanical properties (modulus of 200 kPa and yield stress of 7 kPa); however, the conductivity and interfacial stability were somewhat lowered.[5,7]

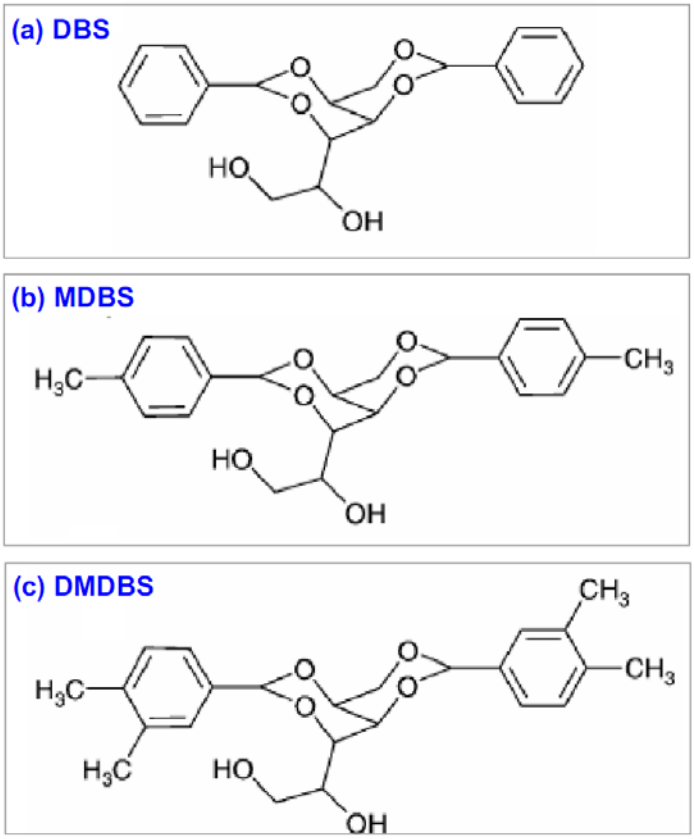

Figure 3.1. Structures of sorbitol-based organogelators: (a) DBS; (b) MDBS; and (c) DMDBS.

Another class of gelling agents for organic solvents are the sorbitol derivatives, 1,3:2,4-di-O-benzylidene-D-sorbitol (DBS) and its variants, 1,3:2,4-di-O-methyl-benzylidene-D-sorbitol (MDBS) and 1,3:2,4-di-O-dimethylbenzylidene-D-sorbitol (DMDBS) (structures of all three are shown in Figure 3.1). DBS is a "butterfly" shaped molecule derived from the sugar alcohol D-glucitol.[22-23] On dissolution in a solvent, these

molecules self organize by hydrogen-bonding into a three-dimensional network of nano-fibrils.[24-28] To our knowledge, very few studies have been published on electrolytes gelled by DBS. [29-30]

In this study, we will examine combinations of DBS derivatives and fumed silica as gelling agents for lithium electrolytes. In particular, we will focus on combinations of MDBS and native FS in an electrolyte formed by dissolving lithium perchlorate ($LiClO_4$) salt in propylene carbonate (PC). Note that the native FS, which has silanol (Si-OH) groups on its particle surfaces, is not capable of gelling PC on its own. On the other hand, MDBS can gel PC, and its gelling ability is superior to those of DBS and DMDBS in the same solvent. The interesting result from our study is that the addition of FS along with MDBS produces a substantially stronger gel in PC compared to that formed by MDBS alone. The MDBS/FS gels are dimensionally stable solids with yield stresses around 15 kPa. At the same time, the ionic conductivities of the gels are identical to those of the parent liquids, i.e., well in excess of 10^{-3} S/cm. Thus, a synergistic effect is observed for mixtures of MDBS/FS with respect to the strength of gels in PC. We have probed the origins of this effect, and a tentative mechanism will be presented based on hydrogen-bonding between the FS particles and the MDBS nano-fibrils.

3.2. EXPERIMENTAL SECTION

Materials. The fumed silica used in this study was kindly supplied by Evonik Degussa Corporation and is available under the trade name, Aerosil 200. This is the native, unmodified fumed silica with a surface covered with silanol (Si-OH) groups. The silanol

groups render the silica hydrophilic, and the silica can consequently be wetted by water. The primary particles of the A200 silica are 12 nm in diameter, and the BET surface area is 200 m^2/g. Prior to use in dispersions, the silica was dried for 24 h in a vacuum oven at 120°C and transferred immediately to an argon-filled glove box. The MDBS was a gift from Milliken Chemicals and were used as received. PC (anhydrous, 99.7%) and $LiClO_4$ (battery grade, dry, 99.99%) were purchased from Sigma-Aldrich. The PC and the $LiClO_4$ were also vacuum-dried for 24 h to remove any adsorbed moisture before being transferred to the glove box.

Sample Preparation. The gel electrolyte samples were prepared in the argon-filled glove box. First a stock solution was made by dissolving $LiClO_4$ in PC in the molar ratio of 1:16. A measured weight of FS was then added to some of the stock electrolyte and dispersed using a high-shear mixer (TissueTearor™, BioSpec Products). The composites were then prepared by weighing the required amount of MDBS in a vial to which the dispersion of FS in $LiClO_4$/PC was added. The mixture was heated with constant stirring on a hot plate till the MDBS dissolved, indicated by the formation of a transparent and homogenous sample. The vial was then taken off the hot-plate and allowed to cool down to room temperature, whereupon the sample turned into a gel. All testing on the gels was done 48 h after their preparation.

Rheological Studies. Dynamic rheological experiments were performed on an AR2000 stress controlled rheometer (TA Instruments). Samples were run on a parallel plate geometry (20 mm dia). A solvent trap was used to minimize contact of the sample with

air and moisture. Dynamic frequency spectra were conducted in the linear viscoelastic regime of the samples, as determined from dynamic strain sweep measurements. Dynamic strain sweeps were conducted at a constant frequency of 1 Hz.

Electrochemical Measurements. Two-electrode coin cells (2032) with stainless steel (SS) or lithium foil (Li) as the blocking and non-blocking electrodes respectively, were used. A stainless steel spacer and spring were used to maintain good contact of electrolyte, electrodes, and current collector.

Conductivity. Conductivity measurements were done using a SS/gel/SS cell by AC impedance spectroscopy over the frequency range 1 Hz to 1 MHz using a Reference 3000 Potentiostat from Gamry Instruments and EIS300 Software for data analysis. An AC signal with amplitude of 10 mV was used. The cells were calibrated at 25°C using a standard KCl solution (1409 μS/cm at 25°C).

Electrochemical Stability Window. Linear sweep voltammetry was used to determine the electrochemical stability window of the sample in a SS/gel/Li cell with the SS disk as the working electrode and the Li foil as the counter electrode. A voltage sweep between 2.5 to 6 V was carried out on the sample at a constant scan rate of 1 mV/s.

Interfacial Stability. An Arbin battery test station was employed to carry out cycling of a Li/gel/Li at a constant current flux of 0.1 mA/cm^2. The direction of the current was reversed every hour and this test was run for 100 cycles. This test was carried out to

investigate the interfacial stability of the gel electrolyte with the lithium metal electrode. Impedance spectroscopy was carried out at various intervals of the galvanostatic cycling.

Transmission Electron Microscopy (TEM). TEM was conducted on a Jeol JEM 2100 microscope at 80 KeV. The staining agent, uranyl acetate (UA) (from Sigma-Aldrich), was dissolved in water to form a 1% stock solution. The hot composite (without the lithium salt) was dropped on carbon/Formvar-coated copper grids immediately after the MDBS had dissolved and before the sample could cool down enough to gel. After letting it stand for 2-3 min, the excess gel was carefully wiped off and the grids were then dried at room temperature. The dried TEM grids were then stained with a drop of the 1% UA solution and air-dried before imaging.

3.3. RESULTS AND DISCUSSION

3.3.1. RHEOLOGICAL STUDIES

The gels under inspection here are four-component systems, where the continuous phase is a solution of $LiClO_4$ in PC, and the dispersed phases are hydrophilic FS and MDBS. Figure 3.2 illustrates the synergistic behavior of MDBS/FS mixtures with respect to gelation. The data shown are from dynamic rheology and are plots of the elastic (G') and viscous (G'') moduli as functions of frequency ω. The responses of three samples are compared in this plot. First, consider the dispersion of 8% FS: in this case, the viscous modulus G'' exceeds the elastic modulus G' over most of the frequency range; moreover, both moduli are strong functions of frequency. Such a response shows that the FS dispersion is a viscous liquid, not a gel, and indeed the sample was visually observed to

be a free-flowing material as well. In comparison, the two MDBS-containing samples both show an elastic, gel-like response: i.e., their $G' > G''$ over the range of frequencies, and moreover, their moduli are relatively independent of frequency.[31] For a given gel, the value of G' reflects the stiffness of the gel network and can be termed the gel modulus. Figure 3.2 shows that the gel modulus of the 2% MDBS + 8% FS gel is about twice that of a gel with 2% MDBS alone. Thus, despite the fact that the FS by itself is not a gelator for PC, it appears to synergistically strengthen the MDBS network. The photograph on the right shows that the MDBS/FS gel is strong enough to support the weight of a spatula that has been stuck in it.

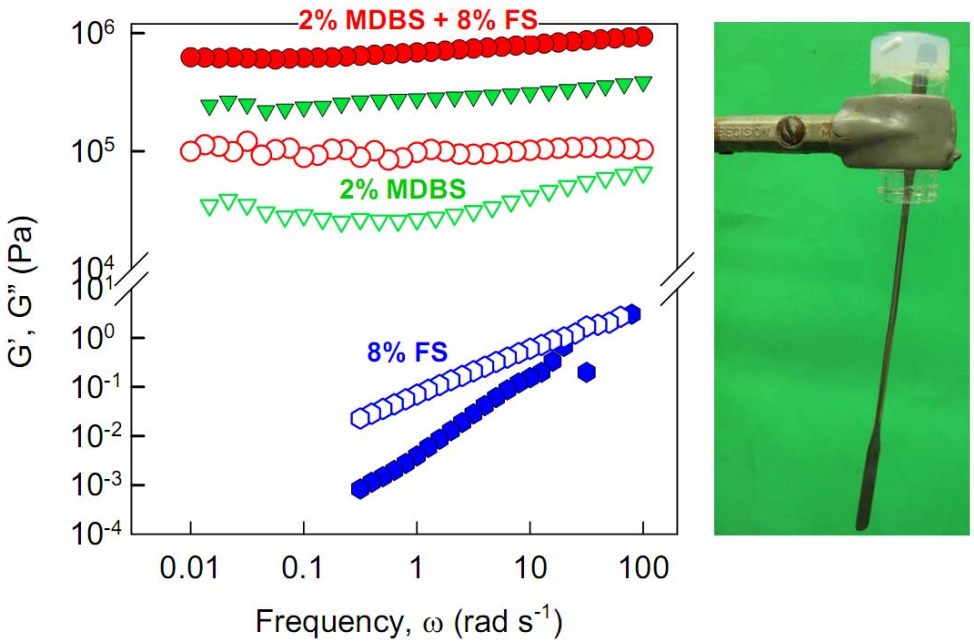

Figure 3.2. Dynamic rheology of three samples in a PC/$LiClO_4$ matrix: **(i)** a 2% MDBS + 8% FS gel (red symbols); **(ii)** a 2% MDBS gel (green symbols); and **(iii)** a 8% FS dispersion (blue symbols). In all cases, the elastic modulus G' is indicated by filled symbols and the viscous modulus G'' by open symbols. The photograph on the right shows the ability of the MDBS/FS gel to hold the weight of a spatula stuck in it.

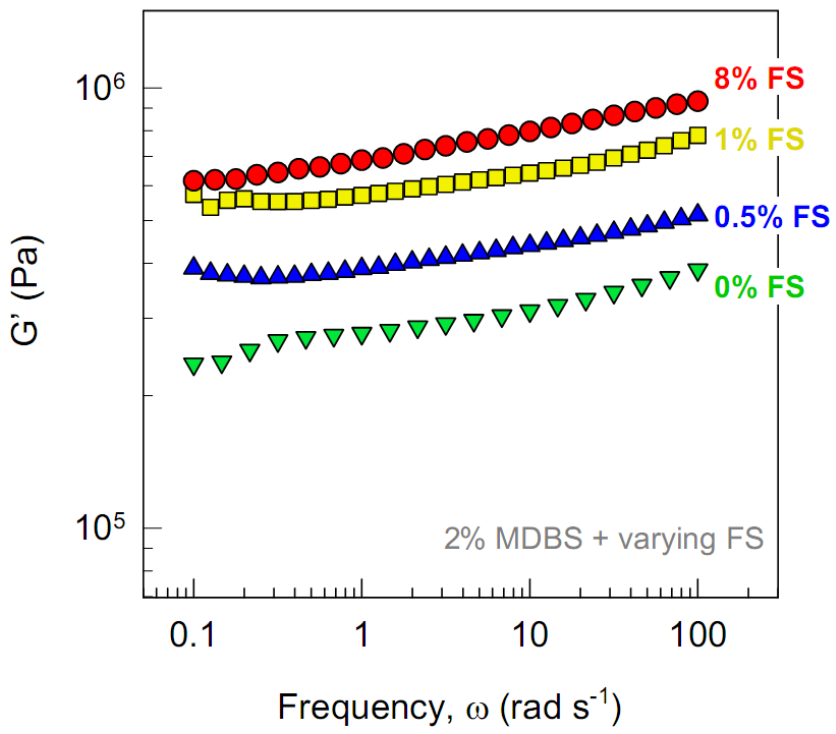

Figure 3.3. Dynamic rheology of samples in a PC/$LiClO_4$ matrix containing 2% MDBS and varying concentrations of FS. All samples were gels; for clarity, only the elastic modulus G' is shown for each sample.

The synergy between MDBS and FS was studied further by varying the FS content for a fixed MDBS content of 2% (Figure 3.3). All the samples were gels, i.e., their G' far exceeded their G'', and so for clarity, only the G' for each sample is shown in the figure. We note that even addition of 0.5% FS enhances the modulus of the 2% MDBS gel by an appreciable amount. A further increase in G' occurs when the FS is raised to 1%, and then the effect more or less saturates, with only a small further enhancement in G' found on raising the FS content to 8%.

It should be noted that the magnitude of G', i.e., the gel modulus, is essentially a measure of the stiffness of the network. This parameter correlates with the density of

cross links in the network structure; however, it does not necessarily imply an increase in gel strength. The key parameter that distinguishes a "strong" gel (e.g., one that can be held between forceps) from a "weak" gel (e.g., one that is a thixotropic, paste-like material) is the yield stress σ_y. This is a measure of the stress it would take to "break" the gel and it is the product of the gel modulus G' and the critical strain γ_y.

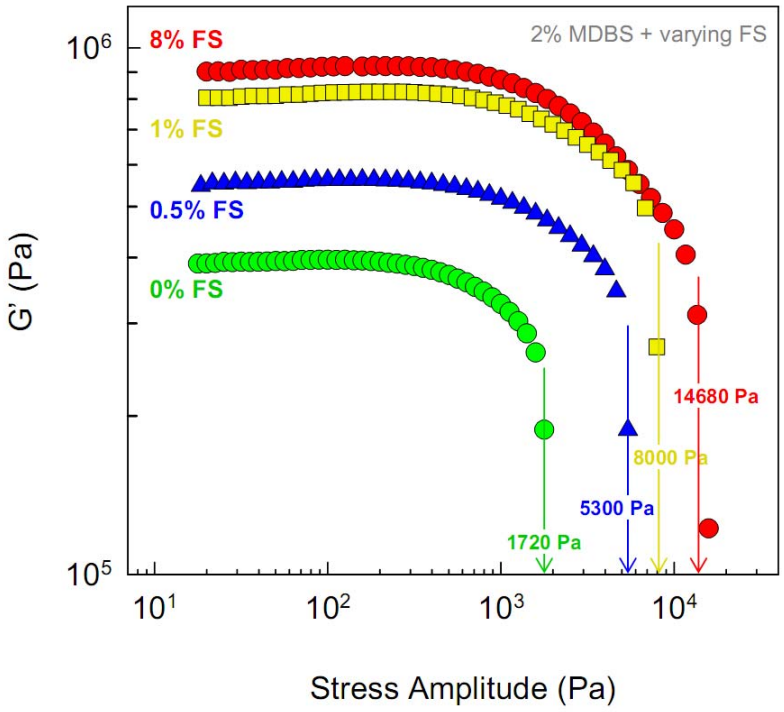

Figure 3.4. Dynamic stress sweeps at 1 Hz for samples in a PC/$LiClO_4$ matrix containing 2% MDBS and varying concentrations of FS. All samples were gels; for clarity, only the elastic modulus G' is shown for each sample. The stress at which G' rapidly plummets is the yield stress σ_y and it is marked by arrows.

One way to determine σ_y is from a dynamic stress sweep experiment, where G' is measured against the stress-amplitude at constant ω. This was conducted for all the samples from Figure 3.3 and indeed the synergistic interaction of MDBS and FS becomes more conspicuous from these data, as shown in Figure 3.4. For each sample, G' follows a

plateau at low stresses and decreases rapidly beyond a certain value of the stress, which is the yield stress σ_y. We estimate σ_y by drawing tangents at the point of rapid decrease in G', as shown by the arrows in Figure 3.4. The results show that σ_y increases almost 10-fold when FS is added to MDBS gels. Note that the 2% MDBS + 8% FS sample has a yield stress σ_y of ~ 15 kPa. This is considerably higher than the σ_y of ~ 7 kPa reported for gel electrolytes made from crosslinkable fumed silica.

3.3.2. ELECTROCHEMICAL STUDIES

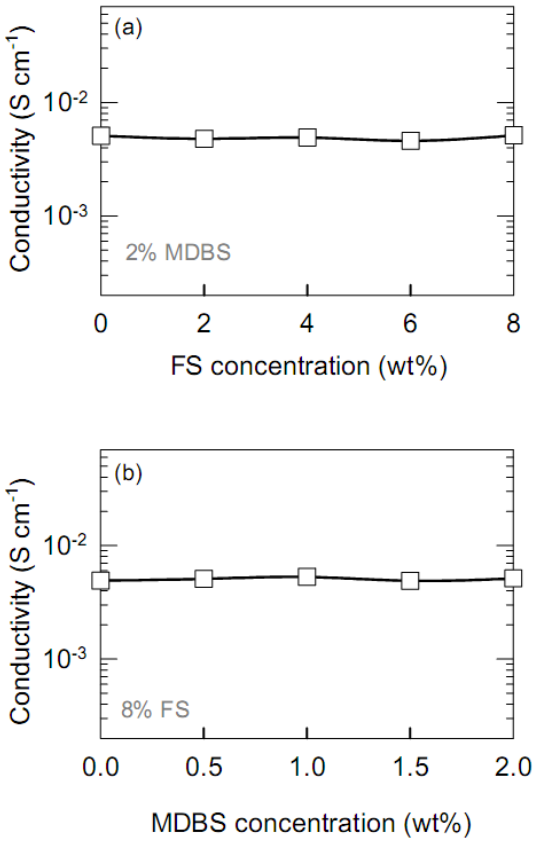

Figure 3.5. Conductivity of PC/$LiClO_4$ electrolytes containing MDBS and FS. **(a)** Effect of varying FS at a constant MDBS concentration of 2%; **(b)** Effect of varying MDBS at a constant FS concentration of 8%.

In addition to the mechanical properties, it is important to determine the electrochemical properties of MDBS/FS-based electrolytes. First, we determined the ionic conductivities of the gel electrolytes, both as a function of FS content at constant MDBS (Figure 3.5a) and as a function of MDBS content at constant FS (Figure 3.5b). In both cases, the conductivity of the gels is unchanged from that of the parent PC/$LiClO_4$ solution, and its value is about 5×10^{-3} S/cm. Thus, it is clear from the data that the gelators do not impair the conductive properties of the electrolytes. As mentioned in the Introduction, the reason for this is probably that the gel networks present in the electrolyte have large pore sizes, thus allowing free diffusion of solvent molecules and ions. The conductivity is thereby decoupled from the gel structure.

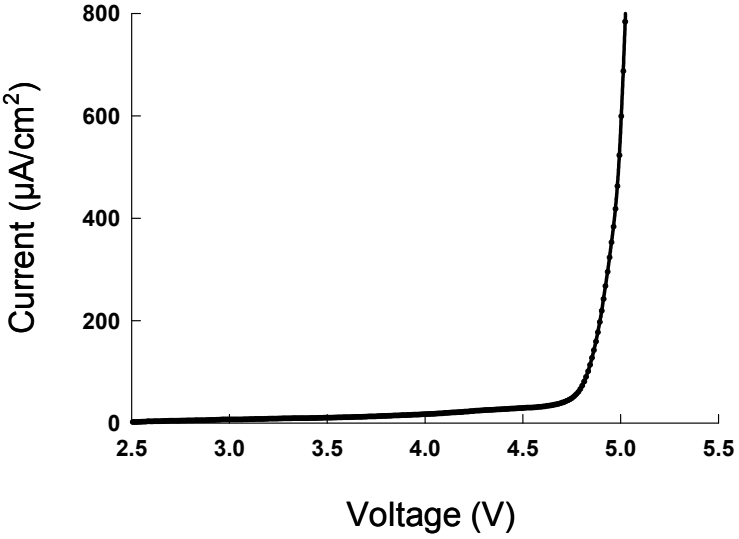

Figure 3.6 Linear sweep voltammetry of a 2% MDBS + 8% FS gel in PC/$LiClO_4$ to find the electrochemical stability window.

It is also important for the electrolyte to have an "electrochemical stability window" that is wide enough to encompass the operating potentials of the electrodes.

Figure 3.6 represents the results of a linear sweep voltammetry scan on the gel electrolyte sandwiched between stainless steel working electrodes. The point where the current rapidly increases in the plot defines the above window. Thus, the gel is seen to show an electrochemical stability window > 4.5 V at room-temperature.

To determine the interfacial stability of the gel electrolyte against lithium, a lithium plating/stripping test was conducted. The electrolyte sample was loaded between two lithium metal electrodes separated by teflon O-rings and the cells so prepared were subjected to a current flux of 0.1 mA/cm^2. The flux was reversed every hour on the hour for 100 cycles. The overvoltage profile (Figure 3.7a) gives a qualitative measure of the stability of the gel with lithium. We note a gradual increase during the first half of the test, while in the latter half there is an unambiguous dip in the overvoltage. This indicates good stability of the gel against the lithium electrode.

Impedance spectroscopy was also conducted on the cells at regular intervals during the galvanostatic cycling. The impedance responses shown in Figure 3.7b are in good agreement with the overvoltage profile. The total resistance of the cell after each cycle is given by the low-frequency data on the impedance plot (i.e., the approximate diameter of the semi-circle measured on the x-axis from the origin). Cycles 10, 20 and 28 show increases in the impedance, which is consistent with the increasing voltage trend in the over-voltage profile. Since the current is constant at 0.1 mA/cm^2, the increase in voltage implies an increase in resistance. The impedance responses after cycles 50, 58 and 78 show a reduction in the total resistance from cycle 28. The responses also nearly

overlap, which implies that the interaction of the electrolyte with the lithium metal electrode has stabilized.

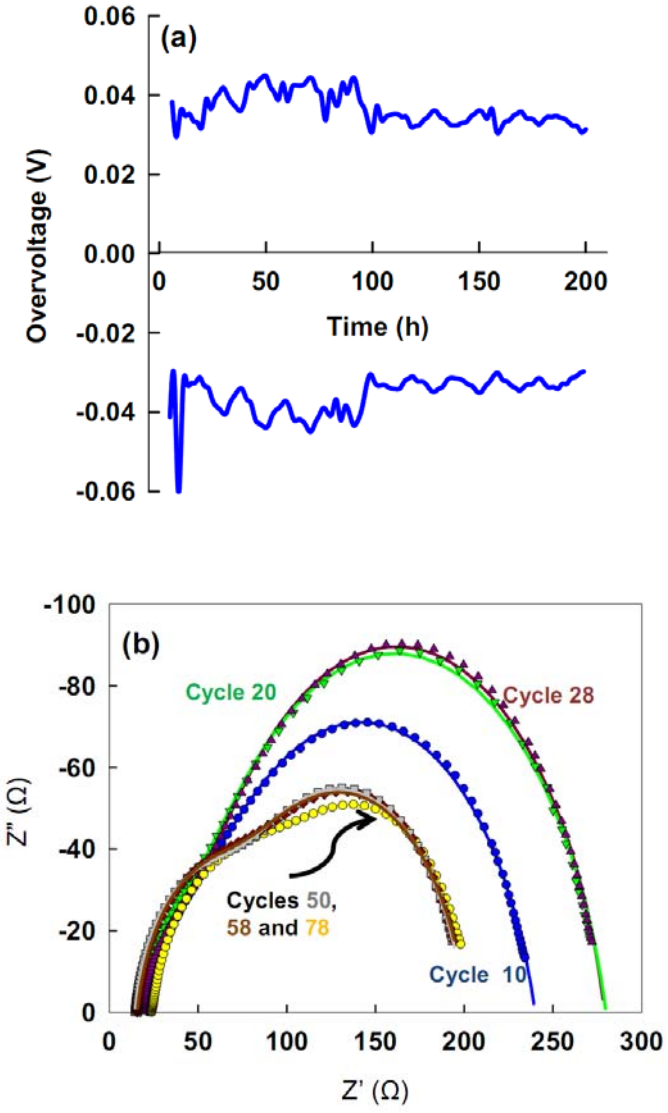

Figure 3.7 Lithium-electrolyte interface stability test conducted at room temperature. **(a)** Overvoltage vs. time profile. **(b)** Impedance response of the cell obtained at the end of various cycles.

To gain insight into the electrolyte stabilization, the impedance scans were fitted to an equivalent circuit. Figure 3.8a illustrates the equivalent circuit that is assumed to mimic the behavior of our cell. The resistance from the ionic conductivity of the

electrolyte is denoted as R_E. The resistance from the passivating film at the solid-electrolyte interface [SEI] is R_{SEI}. Also, during each half-cycle there is a transfer of electrons to the ions to form lithium metal and vice-versa. Thus there is a flow of charge in the cell, and this has its own resistance, which is the charge-transfer resistance R_{CT}. There is also an electrical double layer at the interface which acts like a Constant Phase Element (CPE), represented as a capacitor. The SEI film also has a corresponding CPE. These CPEs are assumed to be in parallel to the R_{SEI} and R_{CT} with all the resistances attached in series, thus giving us the circuit in Figure 3.8a.

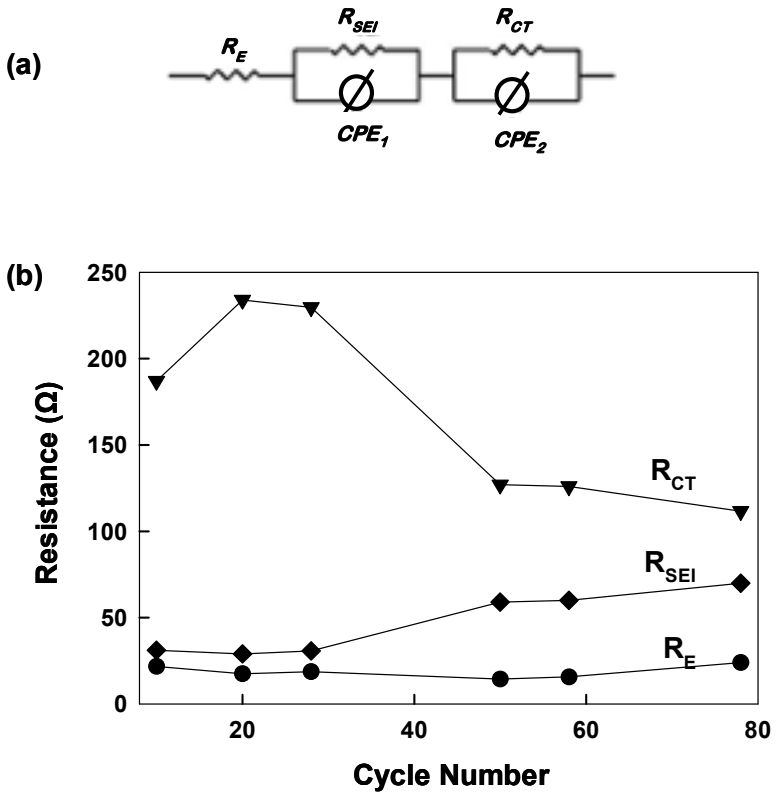

Figure 3.8. (a) Schematic of the equivalent circuit to which the impedance scans in Figure 3.7b were fit. **(b)** Trends in component resistances with increasing cycle number.

The impedance curves in Figure 3.7b are fitted to the above model and the value of the resistance parameters after each cycle are plotted in Figure 3.8b. The ion-conductive resistance R_E is stable during the lithium-interface stability testing. The interfacial resistance R_{SEI} increases gradually, which may be due to the growth of a passivating film. The resistance due to charge transfer R_{CT} decreases considerably midway and then continues to decrease gradually. Altogether, the trends of the resistances suggest that the electrolyte-lithium interface is becoming stabilized by a passivating layer with a relatively low resistance. This combined behavior of the component resistances indicates good stability of the electrolyte with lithium metal.

3.3.3. NANOSTRUCTURAL STUDIES

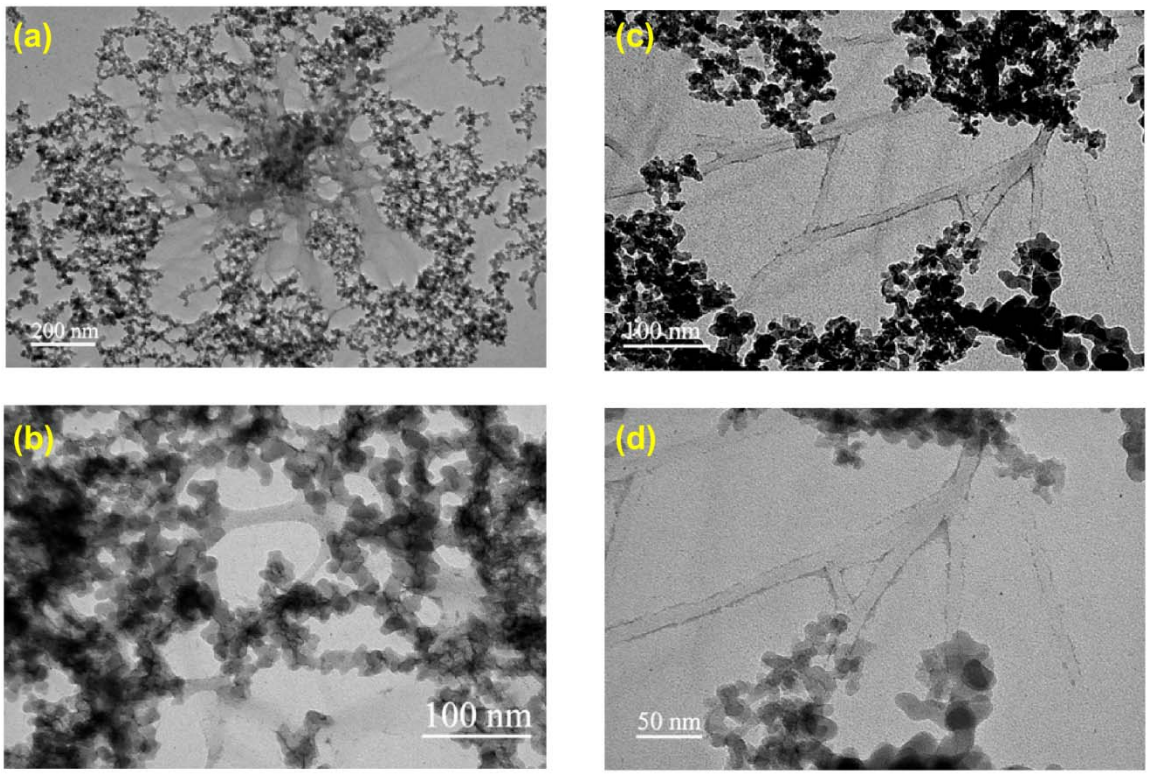

Figure 3.9. TEM images of MDBS-FS gels in PC. The images are stained by uranyl acetate. Branched clusters of FS and nano-fibrils of DBS can both be seen in the images, and the two structures appear to be bound to one another.

Finally, the nanostructure of the gels was studied by TEM to probe the origin of the synergistic gelling behavior. Figure 3.9 shows images of gels stained by uranyl acetate. Numerous branched FS clusters as well as MDBS nano-fibrils with diameters in the range of 10 to 100 nm can be seen. The fibrillar structure is as expected for DBS gels.[22,24-25,32] A key finding from these images is that the FS clusters and the MDBS fibrils appear to be mutually connected and thereby reinforcing each other. For example, in Figure 3.9c and 3.9d, the FS particles appear to be enveloping the MDBS fibrils. In a similar vein, binding of colloidal silica particles to DBS nano-fibrils has been observed in one previous study, where the authors combined the two in poly(ethyl methacrylate).[28]

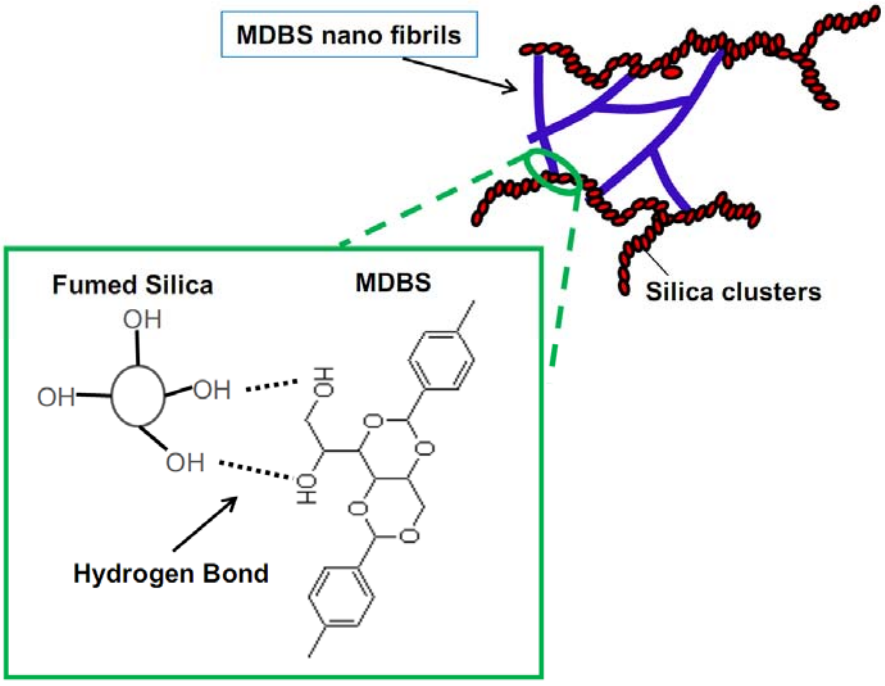

Figure 3.10. Proposed mechanism for explaining the synergistic interaction between MDBS and FS.

In the present case, we can speculate that binding of FS particles to MDBS fibrils occurs through hydrogen-bonding of surface silanols from the FS particles with the free hydroxyls on MDBS molecules/fibrils. Figure 3.10 attempts to illustrate such binding between the two kinds of structures. The additional bonds or crosslinks in the network can explain why the modulus increases in MDBS/FS mixtures compared to that in MDBS alone. It is also possible that when MDBS fibrils are enveloped by FS, they are harder to disrupt via shear, which may explain the increase in the yield stress.

3.4. CONCLUSIONS

We have demonstrated gel electrolytes self assembled from MDBS and FS in a PC/$LiClO_4$ solution. The synergistic interaction between the two additives leads to a mechanically robust electrolyte with a yield stress of ~ 15 kPa and a modulus of around 1000 kPa. At the same time, the gel electrolyte shows good electrochemical properties, including a high ionic conductivity (> 10^{-3} S/cm), a wide electrochemical stability window (> 4.5 V), and good interfacial stability with lithium metal. We believe the synergy between MDBS and FS arises as a result of hydrogen bonding between the polar groups on the two sets of structures. All these properties make this new electrolyte a viable option for use in lithium-ion batteries.

Chapter 4: POLY(ACRYLAMIDE-CO-ACRYLIC ACID) AS A NEW BINDER FOR SILICON ANODES IN LITHIUM-ION BATTERIES.

4.1. INTRODUCTION

A promising energy storage technology today is the lithium-ion battery. Li-ion batteries have shown excellent performance in small portable electronics where the energy requirements are relatively low. Lately, the scope of lithium-ion batteries has been broadened to include the running of hybrid-electric vehicles and electric vehicles, which require high energy storage capacity and high power. For these cases, the usual graphite anode, which has a specific capacity of 372 mAh/g, falls short of practical requirements. This in turn has necessitated a high-capacity substitute for graphite. Silicon (Si) is a promising candidate because it has a theoretical specific capacity of 3579 mAh/g.[3] However, despite its potentially higher capacity, the practical use of Si has been hampered due to its poor cycle stability.

Unlike the mechanism of graphite anodes, where the insertion of Li is of the intercalation type with negligible changes in the graphite structure, the insertion of Li into Si proceeds via formation of alloyed compounds.[33] As a result, there is expansion and contraction of the Si host structure by ~ 300%, as shown by Figure 4.1. Continuous cycling of Si, in turn, rapidly results in mechanical failure and the electrode structure deteriorates. Due to this, the particles in the Si anode break and lose electronic contact with each other, thereby leading to increased electrical resistance. This explains the sub-standard cycling ability of Si.[34-35]

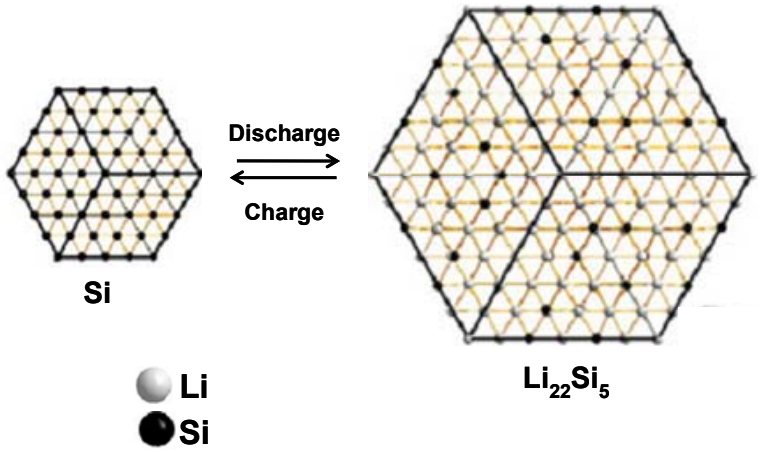

Fig. 4.1 Simplified representation of lithium intercalation into silicon anodes and the resulting volume expansion[36].

In order to realize the full potential of Si as an anode, a solution to avoid the failure of the Si matrix needs to be found. Of the many ideas put forth by research groups, the most elegant and economically feasible option is choosing a good binder. As the name suggests, the job of the binder is to bind the powdered Si particles together and at the same time ensure good adhesion with the underlying current collector. The binder is the inactive component of the anode and yet plays an important role in the functioning of the anode. Significant effort has been put into finding a binder that would work well with Si.[35,37-40] Polyvinylidenefluoride (PVDF), which is the binder of choice for graphite anodes, does not give as good a performance with Si anodes. Instead, the binder that seems to work best is the polymer sodium-carboxymethyl cellulose (CMC).[35,37-40]

Why is CMC an optimal binder for Si anodes? CMC is a rather brittle polymer, and so the fact that it works well suggests that the nature of the bond between the binder and the active material (Si) is probably of key importance. Lestriez et al.[38] suggested that CMC adopts an extended conformation in solution, which enhances the formation of a Si-

CMC network together with conductive carbon black (CB) particles (the latter are usually present in an anode). But these authors still could not explain why CMC would be able to bear a deformation of 300% when its own deformation at break is only 5-8%. Others[36-37] have suggested that an esterification reaction occurs between silanol (Si–OH) groups on Si particles and the carboxylate (COO^-) groups of CMC. (Note that the surface chemistry of Si particles is believed to be identical to that of native silica because Si always undergoes some oxidation to silica at its surface layer.) However, if chemical bonds were being formed between silanols and COO^-, those would restrict the volumetric expansion of the composite. Bridel et al.[41] therefore proposed that the CMC-Si bond is of the self-healing hydrogen-bonding (H-bonding) type. Such a bond would not only have enough strength to maintain the structure and electrical contact but also be weak enough to break under mechanical stress allowing the full lithiation of Si.

CMC is a linear derivative of cellulose (see structure in Figure 4.2a). While cellulose is insoluble in water, the hydrophilic carboxymethyl groups facilitate the aqueous dissolution of CMC. Note that the PVDF binder used with graphite anodes is insoluble in water and requires the use of N-methyl pyrrolidinone (NMP) as a solvent. This not only adds to the cost of production of Li-ion batteries but also poses an environmental and safety hazard. The cheapness of CMC, its solubility in water, and most importantly its ability to accommodate the volumetric expansion of Si make it a viable candidate for commercial Si anodes.

This Chapter reports a study on poly(acrylamide-co-acrylic acid) (PAmA), which is another water-soluble binder for use with Si anodes. PAmA is a copolymer of acrylamide and acrylic acid, and its structure is shown in Figure 4.2b. It is used industrially as a thickening agent, filtering aid, or flocculating agent. We will show that PAmA performs as well as CMC in some cases and better than CMC in other cases. We also study the effect of polymer molecular weight (MW) on the performance of this binder.[41] Low-MW poly(acrylic acid) (PAA) has been studied as binder for Si anodes and has shown an increase in adhesion strength but no improvement in room-temperature discharge capacity[41-42] while higher MW of PAA has shown promising results as a binder for graphite anodes.[43-44] However the PAmA copolymer has not been tested as a binder with Si anodes to the best of our knowledge. We chose this binder because its carboxylic acid (–COOH) and amine ($–NH_2$) groups could potentially provide H-bonding sites for the interaction of Si–OH groups on the surfaces of Si particles.

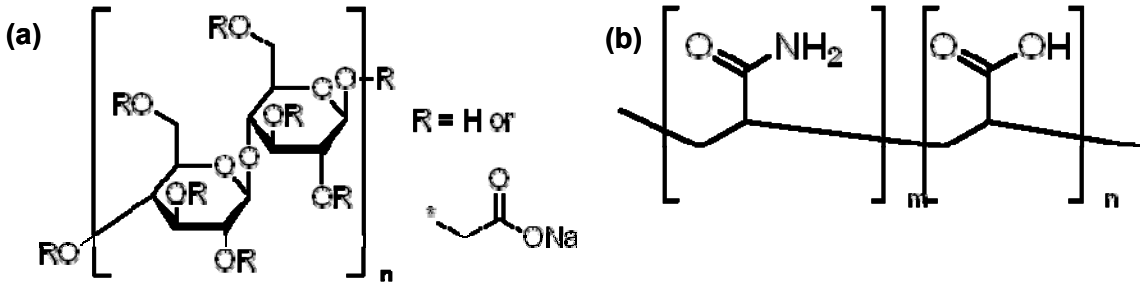

Figure 4.2. Structure of **(a)** carboxymethyl cellulose (CMC); and **(b)** poly(acrylamide-co-acrylic acid) (PAmA). [45]

4.2. EXPERIMENTAL SECTION

Materials. Si nanoparticles (≥ 98%, average size 50 nm) were purchased from Sigma-Aldrich. Blended carbon black (denoted CB) particles were used as the conductive additive. Two CMC binders differing in their molecular weights (90,000 g/mol and 700,000 g/mol) were purchased from Sigma-Aldrich. They will be referred to as L-CMC and H-CMC respectively. Similarly, two PAmA binders differing in molecular weights (200,000 g/mol and 5,000,000 g/mol) were also purchased from Sigma-Aldrich. They will be referred to as L-PAmA and H-PAmA, respectively. Particles and polymers were used as received.

Electrode Preparation. Measured amounts of Si particles, CB particles, and binder were weighed into an egg-shaped stainless steel vial. A small amount of de-ionized water was introduced to give the slurry a suitable viscosity. The slurry was milled in a Fritsch Pulverisette 6 mixer for 3 h with zirconia balls as the milling media. The milled slurry was then cast on a copper foil (current collector) using a notch bar. The thickness of the film cast was 60 μm. After allowing the slurry to dry overnight, it was placed in a vacuum oven for 24 h at 120°C for further drying. Electrodes of 1.27 cm dia were punched from the dried material and transferred to an argon-filled glove box. Three different compositions of electrodes were prepared: (i) 80% Si, 10% CB, 10% binder (ii) 60% Si, 10% CB 30% binder and (iii) 33% Si, 33% CB, 33% binder (all % are by wt.).

Electrochemical Characterization. For the electrochemical analysis, two-electrode coin cells (2032) with lithium foil as counter electrode were used. An electrolyte of 1 M

lithium hexafluorophosphate ($LiPF_6$) was prepared in a mixed solution of ethylene carbonate (EC) and diethyl carbonate DEC (1:1 by volume). The anode of interest, the above electrolyte, and a micro-porous separator (Celgard®3501) were combined to form the cell. The cells were discharged and charged at 500 mAh/g between 0 V and 1.5 V (vs. Li/Li^+) using an Arbin battery test station.

4.3. Results and Discussion

4.3.1. 80% Si, 10% CB, 10% binder

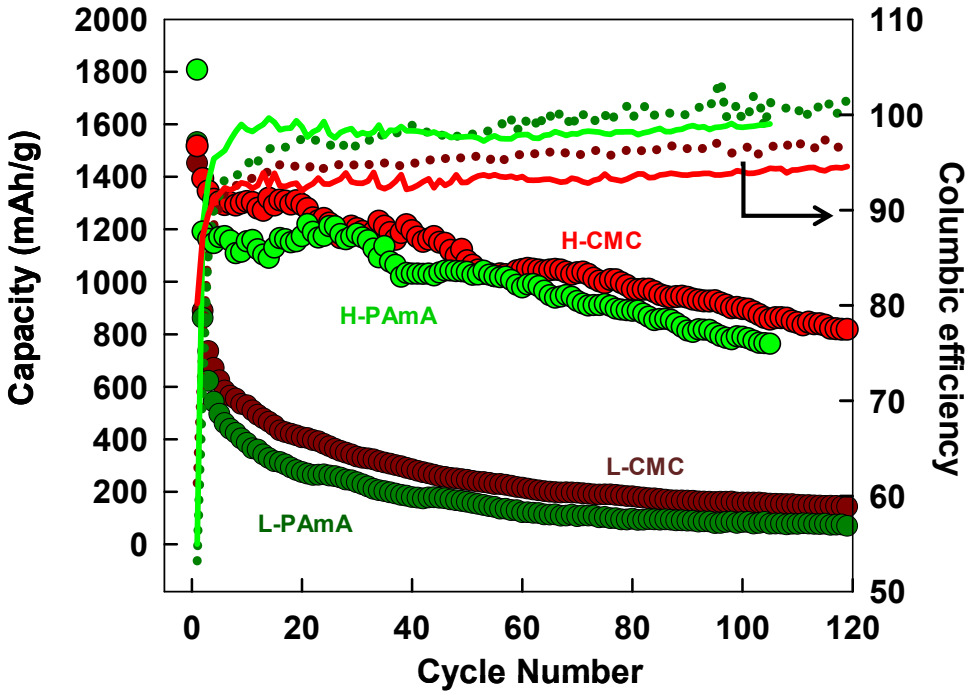

Figure 4.3. Capacity vs. cycle number for a composition of 80% Si, 10% CB and 10% binder. Results are shown for four binders (two MWs of CMC, two MWs of PAmA).

Figure 4.3 shows the results of cycling studies conducted with an anode composed of 80% Si particles, 10% CB particles and 10% binder. At such a high

concentration of active material (i.e., Si), the anodes are expected to show good first lithiation capacity but large subsequent reductions in capacity.[41 46] The low MW binder-based anodes conform with the expected results, but curiously, their high MW counterparts show good performance, albeit with a slow and steady capacity fade. The H-PAmA composite shows a first lithiation capacity of 1800 mAh/g and still manages to retain almost 900 mAh/g after 100 cycles. This is encouraging since its performance is similar to that of the tried and tested H-CMC. All the samples tested showed an efficiency of less than 95%. The capacity fade is probably due to the large volume expansion of silicon.[47] When the Si particles expand and contract by 300%, a lot of particle displacement would occur. Some Si particles may get displaced to an extent that they are no longer in contact with the CB, and those particles would then get electronically isolated from the bulk electrode, which explains the capacity fade.

4.3.2. 60% Si, 10% CB, 30% binder

Next, we increased the content of binder to 30% while keeping the CB at 10%. The Si content was thus reduced to 60% Si. Figure 4.4 shows the cycling results for these electrodes. The L-PAmA shows a high initial lithiation capacity of 1800 mAh/g and then a large capacity loss within the first 10 cycles. Thereafter, the capacity fade is slow but it still retains a capacity of 500 mAh/g after 110 cycles with cycling efficiency of 97%. Both the H-PAmA and H-CMC composites show almost identical trends with initial lithiation capacity of around 1400 mAh/g and then cycling down to about 300 mAh/g with an efficiency of 98%. The L-CMC sample shows a sudden drop in capacity in the first 5 cycles itself and after that gives a modest cycling performance to 300 mAh/g with

efficiency of 96%. The overall characteristic pattern of a good start followed by a bad finish for these electrodes is attributed to the low CB and high binder content, which tends to insulate the active Si particles. Thus, the Si particles lose electronic contact during cycling, resulting in the eventual capacity fade.

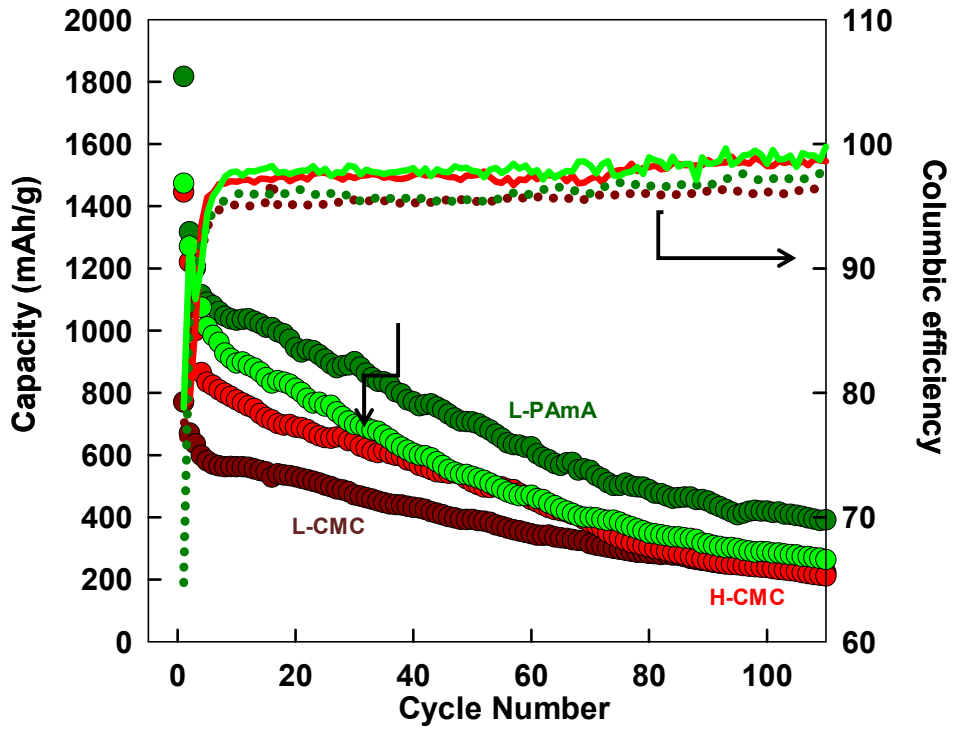

Figure 4.4. Capacity vs. cycle number for a composition of 60% Si, 10% CB and 30% binder. Results are shown for four binders (two MWs of CMC, two MWs of PAmA).

4.3.3. 33% SILICON 33% CARBON BLACK 33%BINDER

Finally, we studied a composition of 33% Si, 33% CB and 33% binder. Figure 4.5 shows the cycling results for the corresponding electrodes. In this case, the L-PAmA performs the best, surpassing both the H-CMC and the H-PAmA. Both L-PAmA and H-CMC show a first cycle discharge of 2900 mAh/g. After 110 cycles, the L-PAmA

shows a capacity of 1200 mAh/g while the H-CMC shows a capacity of 1000 mAh/g. The above performance of the HCMC is in agreement with the data of Bridel et al.[41], who also used the CMC with an MW of 700,000 g/mol. The H-PAmA shows an initial lithiation of nearly 2800 mAh/g but curiously, has a large capacity loss and drops to around 1700 mAh/g during the 2nd cycle. Although its efficiency is low relative to the other samples, it still manages to retain up to 500 mAh/g after 110 cycles. L-CMC shows an initial capacity of 1500 mAh/g and then cycles down to 500 mAh/g after 110 cycles. The L-CMC, H-CMC, and L-PAmA all cycle with an efficiency ≈ 99%.

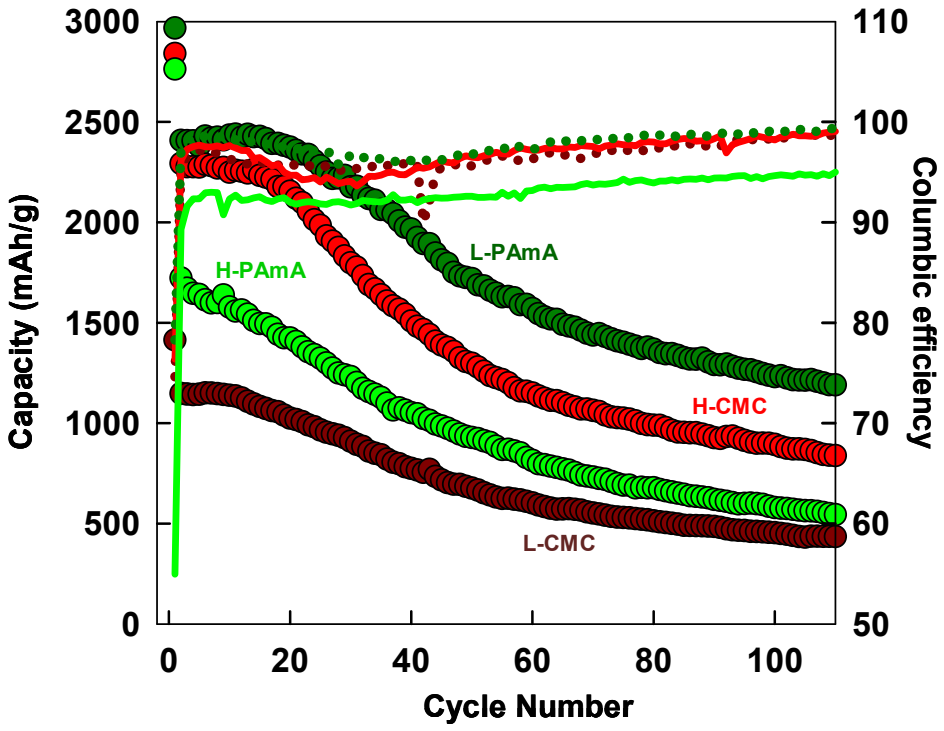

Figure 4.5. Capacity vs. cycle number for a composition of 33% Si, 33% CB and 33% binder. Results are shown for four binders (two MWs of CMC, two MWs of PAmA).

Altogether, we note the excellent cycling performance of the L-PAmA and HCMC at this composition. It appears that the low wt% of Si particles allows for their

freer expansion while lithium insertion occurs. If particle displacement occurs, the high CB content ensures that electrical contact is maintained. Also, the relatively high concentration of binder is able to prevent the structure from disintegrating.

We should mention here that other research groups[35,48] have obtained better performance with the CMC binder by controlling the lower limit of the voltage during cycling. As suggested by Obrovac et al.[49], the low voltage prevents the crystallization of the Si particles. However, this is not practical in real-world applications of Si anodes as the degree to which a cell will be discharged cannot be controlled. Therefore, studies conducted here have been under the stringent condition of cycling between 0 V to 1.5 V.

4.4. CONCLUSIONS

In this Chapter, we have studied poly(acrylamide-co-acrylic acid) (PAmA) as a binder for high-capacity Si anodes, and compared its performance with that of the industry standard, CMC. Two MWs each of the PAmA and CMC were tested. At high concentrations of Si particles (60%), the high MW binders out-performed their low MW counterparts. On the other hand, at a composition with equal amounts (33%) of Si, binder, and CB, the low MW PAmA out-performed even the high MW CMC and exhibited an efficiency near 99%. A limitation of the new binder, which is also the case for CMC, is the continuous capacity fade. This limitation impedes its commercialization, but the results presented here at least show the potential of PAmA to serve as a viable alternative to CMC as a binder within silicon anodes.

Chapter 5: CONCLUSIONS AND RECOMMENDATIONS.

5.1. CONCLUSIONS

The principle motive behind this thesis is the development of novel materials for the over-all enhancing of performance of lithium-ion batteries. Two separate studies were conducted with a view to enhance the respective properties of electrolytes and silicon anodes.

In the first study on solid-gel electrolytes the key point that has been unearthed is that gelation of electrolytic liquids can occur through the use of more than one gelator. Rheological and electrochemical studies were conducted on the gel electrolytes to confirm that the mechanical strength was indeed enhanced by the synergy phenomenon between two gelators and that the electrochemical properties of the electrolyte were largely unaffected.

In the second study, discovery of a new binder was attempted. This particular choice of a binder to be tried was made due to its long chain size and the free sites available for hydrogen bonding. The results of this study showed that poly (acrylamide-co-acrylic acid) does indeed perform very well with silicon anode for more than 100 cycles and has the potential to out-run CMC as the benchmark binder for high capacity anodes.

5.2. FUTURE DIRECTIONS

Future work on the subject of electrolyte could involve varying the type of fumed silica and the DBS derivative used. Since high concentrations of monomers are required for ensuring a strong gel with cross linkable fumed silica which affects the conductivity and lithium interface stability due to unreacted monomer, using it in conjugation with a DBS gelator may reduce the amount of monomer required to induce cross linking and could increase the mechanical strength more than the current system.

For future work on the new binder, morphological studies will need to be done to understand the interaction with silicon at smaller length scales to explain what makes this binder potentially better than CMC. The pH of the composite may be varied to optimize the conditions under which poly (acrylamide-co-acrylic acid) will give its best performance. If it can be decisively concluded that the performance is due to the hydrogen bonding as suspected with CMC then other long chain, water soluble polymers with free hydrogen bonding sites could be tried.

REFERENCES

[1] Scrosati, B. "Nanomaterials - Paper powers battery breakthrough." *Nature Nanotechnology* **2007**, *2*, 598-599.

[2] Lee, H. H.; Wan, C. C.; Wang, Y. Y. "Identity and thermodynamics of lithium intercalated in graphite." *Journal of Power Sources* **2003**, *114*, 285-291.

[3] Obrovac, M. N.; Christensen, L. "Structural changes in silicon anodes during lithium insertion/extraction." *Electrochemical and Solid State Letters* **2004**, *7*, A93-A96.

[4] Energy Efficiency and Renewable Energy, U. S. Dept. of Energy. *www.eere.energy.gov*

[5] Yerian, J. A.; Khan, S. A.; Fedkiw, P. S. "Crosslinkable fumed silica-based nanocomposite electrolytes: role of methacrylate monomer in formation of crosslinked silica network." *Journal of Power Sources* **2004**, *135*, 232-239.

[6] Walkowiak, M.; Zalewska, A.; Jesionowski, T.; Waszak, D.; Czajka, B. "Effect of chemically modified silicas on the properties of hybrid gel electrolyte for Li-ion batteries." *Journal of Power Sources* **2006**, *159*, 449-453.

[7] Li, Y. X.; Yerian, J. A.; Khan, S. A.; Fedkiw, P. S. "Crosslinkable fumed silica-based nanocomposite electrolytes for rechargeable lithium batteries." *Journal of Power Sources* **2006**, *161*, 1288-1296.

[8] Choi, B. K.; Kim, Y. W.; Shin, K. H. "Effects of ceramic fillers on the electrical properties of (PEO)(16)LiClO4 electrolytes." *Journal of Power Sources* **1997**, *68*, 357-360.

[9] Croce, F.; Curini, R.; Martinelli, A.; Persi, L.; Ronci, F.; Scrosati, B.; Caminiti, R. "Physical and chemical properties of nanocomposite polymer electrolytes." *Journal of Physical Chemistry B* **1999**, *103*, 10632-10638.

[10] Appetecchi, G. B.; Scaccia, S.; Passerini, S. "Investigation on the stability of the lithium-polymer electrolyte interface." *Journal of the Electrochemical Society* **2000**, *147*, 4448-4452.

[11] Appetecchi, G. B.; Croce, F.; Persi, L.; Ronci, F.; Scrosati, B. "Transport and interfacial properties of composite polymer electrolytes." *Electrochimica Acta* **2000**, *45*, 1481-1490.

[12] Capuano, F.; Croce, F.; Scrosati, B. "Composite Polymer Electrolytes." *Journal of the Electrochemical Society* **1991**, *138*, 1918-1922.

[13] Song, J. Y.; Wang, Y. Y.; Wan, C. C. "Review of gel-type polymer electrolytes for lithium-ion batteries." *Journal of Power Sources* **1999**, *77*, 183-197.

[14] Ballard, D. G. H.; Cheshire, P.; Mann, T. S.; Przeworski, J. E. "Ionic-Conductivity in Organic-Solids Derived from Amorphous Macromolecules." *Macromolecules* **1990**, *23*, 1256-1264.

[15] Hou, J.; Baker, G. L. "Preparation and characterization of cross-linked composite polymer electrolytes." *Chemistry of Materials* **1998**, *10*, 3311-3318.

[16] Zhou, J.; Fedkiw, P. S.; Khan, S. A. "Interfacial stability between lithium and fumed silica-based composite electrolytes." *Journal of the Electrochemical Society* **2002**, *149*, A1121-A1126.

[17] Walls, H. J.; Zhou, J.; Yerian, J. A.; Fedkiw, P. S.; Khan, S. A.; Stowe, M. K.; Baker, G. L. "Fumed silica-based composite polymer electrolytes: synthesis, rheology, and electrochemistry." *Journal of Power Sources* **2000**, *89*, 156-162.

[18] Fan, J.; Fedkiw, P. S. "Composite electrolytes prepared from fumed silica, polyethylene oxide oligomers, and lithium Salk." *Journal of the Electrochemical Society* **1997**, *144*, 399-408.

[19] Fan, J.; Raghavan, S. R.; Yu, X. Y.; Khan, S. A.; Fedkiw, P. S.; Hou, J.; Baker, G. L. "Composite polymer electrolytes using surface-modified fumed silicas: conductivity and rheology." *Solid State Ionics* **1998**, *111*, 117-123.

[20] Khan, S. A.; Baker, G. L.; Colson, S. "Composite Polymer Electrolytes Using Fumed Silica Fillers - Rheology and Ionic-Conductivity." *Chemistry of Materials* **1994**, *6*, 2359-2363.

[21] Zhou, H.; Fedkiw, P. S. "Cycling of lithium/metal oxide cells using composite electrolytes containing fumed silicas." *Electrochimica Acta* **2003**, *48*, 2571-2582.

[22] Mercurio, D. J.; Spontak, R. J. "Morphological characteristics of 1,3 : 2,4-dibenzylidene sorbitol/poly(propylene glycol) organogels." *Journal of Physical Chemistry B* **2001**, *105*, 2091-2098.

[23] Chen, W. Y.; Yang, Y. J.; Lee, C. H.; Shen, A. Q. "Confinement effects on the self-assembly of 1,3 : 2,4-di-p-methylbenzylidene sorbitol based organogel." *Langmuir* **2008**, *24*, 10432-10436.

[24] Yamasaki, S.; Tsutsumi, H. "Microscopic Studies of 1,3-2,4-Di-O-Benzylidene-D-Sorbitol in Ethylene-Glycol." *Bulletin of the Chemical Society of Japan* **1994**, *67*, 906-911.

[25] Yamasaki, S.; Tsutsumi, H. "The Dependence of the Polarity of Solvents on 1,3/2,4-Di-O-Benzylidene-D-Sorbitol Gel." *Bulletin of the Chemical Society of Japan* **1995**, *68*, 123-127.

[26] Watase, M.; Itagaki, H. "Thermal and rheological properties of physical gels formed from benzylidene-D-sorbitol derivatives." *Bulletin of the Chemical Society of Japan* **1998**, *71*, 1457-1466.

[27] Watase, M.; Nakatani, Y.; Itagaki, H. "On the origin of the formation and stability of physical gels of di-O-benzylidene-D-sorbitol." *Journal of Physical Chemistry B* **1999**, *103*, 2366-2373.

[28] Wilder, E. A.; Braunfeld, M. B.; Jinnai, H.; Hall, C. K.; Agard, D. A.; Spontak, R. J. "Nanofibrillar networks in poly(ethyl methacrylate) and its silica nanocomposites." *Journal of Physical Chemistry B* **2003**, *107*, 11633-11642.

[29] Nahir, T. M.; Qiu, Y. J.; Williams, J. L. "Electrochemical Characterization of a Novel Organic Electrolyte Gel." *Electroanalysis* **1994**, *6*, 972-975.

[30] Mohmeyer, N.; Wang, P.; Schmidt, H. W.; Zakeeruddin, S. M.; Gratzel, M. "Quasi-solid-state dye sensitized solar cells with 1,3 : 2,4-di-O-benzylidene-D-sorbitol derivatives as low molecular weight organic gelators." *Journal of Materials Chemistry* **2004**, *14*, 1905-1909.

[31] Raghavan, S. R.; Riley, M. W.; Fedkiw, P. S.; Khan, S. A. "Composite polymer electrolytes based on poly(ethylene glycol) and hydrophobic fumed silica: Dynamic rheology and microstructure." *Chemistry of Materials* **1998**, *10*, 244-251.

[32] Wilder, E. A.; Hall, C. K.; Khan, S. A.; Spontak, R. J. "Effects of composition and matrix polarity on network development in organogels of poly(ethylene glycol) and dibenzylidene sorbitol." *Langmuir* **2003**, *19*, 6004-6013.

[33] Carmer, J. L. G.; Morales, J.; Sanchez, L. "Nano-Si/cellulose composites as anode materials for lithium-ion batteries." *Electrochemical and Solid State Letters* **2008**, *11*, A101-A104.

[34] Chen, Z. H.; Christensen, L.; Dahn, J. R. "Large-volume-change electrodes for Li-ion batteries of amorphous alloy particles held by elastomeric tethers." *Electrochemistry Communications* **2003**, *5*, 919-923.

[35] Buqa, H.; Holzapfel, M.; Krumeich, F.; Veit, C.; Novak, P. "Study of styrene butadiene rubber and sodium methyl cellulose as binder for negative electrodes in lithium-ion batteries." *Journal of Power Sources* **2006**, *161*, 617-622.

[36] Ding, N.; Xu, J.; Yao, Y. X.; Wegner, G.; Lieberwirth, I.; Chen, C. H. "Improvement of cyclability of Si as anode for Li-ion batteries." *Journal of Power Sources* **2009**, *192*, 644-651.

[37] Hochgatterer, N. S.; Schweiger, M. R.; Koller, S.; Raimann, P. R.; Wohrle, T.; Wurm, C.; Winter, M. "Silicon/graphite composite electrodes for high-capacity anodes: Influence of binder chemistry on cycling stability." *Electrochemical and Solid State Letters* **2008**, *11*, A76-A80.

[38] Lestrie, B.; Bahri, S.; Sandu, I.; Roue, L.; Guyomard, D. "On the binding mechanism of CMC in Si negative electrodes for Li-ion batteries." *Electrochemistry Communications* **2007**, *9*, 2801-2806.

[39] Baranchugov, V.; Markevich, E.; Pollak, E.; Salitra, G.; Aurbach, D. "Amorphous silicon thin films as a high capacity anodes for Li-ion batteries in ionic liquid electrolytes." *Electrochemistry Communications* **2007**, *9*, 796-800.

[40] Liu, W. R.; Yang, M. H.; Wu, H. C.; Chiao, S. M.; Wu, N. L. "Enhanced cycle life of Si anode for Li-ion batteries by using modified elastomeric binder." *Electrochemical and Solid State Letters* **2005**, *8*, A100-A103.

[41] Bridel, J. S.; Azais, T.; Morcrette, M.; Tarascon, J. M.; Larcher, D. "Key Parameters Governing the Reversibility of Si/Carbon/CMC Electrodes for Li-Ion Batteries." *Chemistry of Materials* **2010**, *22*, 1229-1241.

[42] Lee, J. H.; Paik, U.; Hackley, V. A.; Choi, Y. M. "Effect of poly(acrylic acid) on adhesion strength and electrochemical performance of natural graphite negative electrode for lithium-ion batteries." *Journal of Power Sources* **2006**, *161*, 612-616.

[43] Komaba, S.; Okushi, K.; Ozeki, T.; Yui, H.; Katayama, Y.; Miura, T.; Saito, T.; Groult, H. "Polyacrylate Modifier for Graphite Anode of Lithium-Ion Batteries." *Electrochemical and Solid State Letters* **2009**, *12*, A107-A110.

[44] Komaba, S.; Yabuuchi, N.; Ozeki, T.; Okushi, K.; Yui, H.; Konno, K.; Katayama, Y.; Miura, T. "Functional binders for reversible lithium intercalation into graphite in propylene carbonate and ionic liquid media." *Journal of Power Sources* **2010**, *195*, 6069-6074.

[45] Sigma-Aldrich. *www.sigmaaldrich.com*.

[46] Beattie, S. D.; Larcher, D.; Morcrette, M.; Simon, B.; Tarascon, J. M. "Si electrodes for li-ion batteries - A new way to look at an old problem." *Journal of the Electrochemical Society* **2008**, *155*, A158-A163.

[47] Timmons, A.; Dahn, J. R. "In situ optical observations of particle motion in alloy negative electrodes for Li-ion batteries." *Journal of the Electrochemical Society* **2006**, *153*, A1206-A1210.

[48] Li, J.; Lewis, R. B.; Dahn, J. R. "Sodium carboxymethyl cellulose - A potential binder for Si negative electrodes for Li-ion batteries." *Electrochemical and Solid State Letters* **2007**, *10*, A17-A20.

[49] Obrovac, M. N.; Krause, L. J. "Reversible cycling of crystalline silicon powder." *Journal of the Electrochemical Society* **2007**, *154*, A103-A108.